Photoelectron angular distributions from strong-field ionization of oriented molecules

Lotte Holmegaard[1], Jonas L. Hansen[2], Line Kalhøj[1], Sofie Louise Kragh[1], Henrik Stapelfeldt[1,2]*, Frank Filsinger[3], Jochen Küpper[3], Gerard Meijer[3], Darko Dimitrovski[4], Mahmoud Abu-samha[4], Christian P. J. Martiny[4] and Lars Bojer Madsen[4]*

The combination of ultrafast light sources with detection of molecular-frame photoelectron angular distributions (MF-PADs) is setting new standards for detailed interrogation of molecular dynamics[1-8]. However, until recently measurement of MFPADs relied on determining the molecular orientation after ionization[1,9-13], which is limited to species and processes where ionization leads to fragmentation. An alternative is to fix the molecular frame before ionization. The only demonstrations of such spatial orientation involved aligned small linear nonpolar molecules[5,6,14]. Here we extend these techniques to the general class of polar molecules. Carbonylsulphide and benzonitrile molecules, fixed in space by combined laser and electrostatic fields, are ionized with intense, circularly polarized 30-fs laser pulses. For carbonylsulphide and benzonitrile oriented in one dimension, the MFPADs exhibit pronounced anisotropies perpendicular to the fixed permanent dipole moment, which are absent for randomly oriented molecules. Furthermore, for benzonitrile oriented in three dimensions, striking suppression of electron emission in the fixed molecular plane appears. Our theoretical analysis, based on tunnelling ionization theory[15,16], shows that the MFPADs reflect permanent dipole moments and polarizabilities of both the neutral molecule and its cation, and nodal planes of occupied electronic orbitals. These results point to future opportunities for time-resolved probing of valence electron dynamics.

Experimentally a target of adiabatically aligned and oriented molecules is created by the combined action of a 10 ns laser pulse and a weak static electric field[17,18]. Here, alignment refers to confinement of molecule-fixed axes along laboratory-fixed axes, and orientation refers to the molecular dipole moment pointing in a particular direction[19]. Before reaching the interaction point with the laser pulses and the static field the molecules are selected in the lowest-lying rotational quantum states by an electrostatic deflector[20]. Hereby, alignment and orientation is optimized, which is crucial for observation of the MFPAD effects discussed next. The degree of alignment and orientation is initially measured by Coulomb exploding the molecules using an intense femtosecond probe laser pulse (Supplementary Information).

For the photoelectron angular distribution (PAD) experiments, a circularly polarized, 30 fs probe pulse, centred at 800 nm, is used. First, the linear carbonylsulphide (OCS) molecule is studied. At a peak intensity $\simeq 2.4 \times 10^{14}$ W cm^{-2}, OCS undergoes only single ionization with essentially no fragmentation. The

intensity puts the dynamics in the tunnelling regime[21] (see Supplementary Information) and the circular polarization ensures that no recollision of the freed electron with its parent ion occurs. Both conditions are important for the interpretation and modelling of the observed PADs. The linear polarization of the alignment laser is parallel to the static field axis (Fig. 1a). Hereby, the OCS molecules are strongly confined along this axis with a degree of orientation corresponding to about 80% of the molecules having their O-end facing the detector and 20% facing oppositely.

The electron images are shown in Fig. 1. Applying only the probe pulse (Fig. 1b,c) the electrons emerge in a stripe parallel to the polarization plane (y, z) of the probe pulse for both left and right circularly polarized (LCP and RCP) pulses. When the molecules are one-dimensional aligned, and oriented as shown in Fig. 1a, a strong up–down asymmetry is observed (Fig. 1d,e). The asymmetry reverses as the helicity of the probe pulses is flipped. For LCP (RCP) probe pulses, the number of electrons detected in the upper part compared with the total number in the image is ~64% (39%). Without the alignment pulse, only a very weak asymmetry is seen. It may result from very mild alignment and orientation owing to the interaction between the permanent dipole moment and the static field[22].

To explain the experimental findings we model the ionization process by modified tunnelling theory. The model (Supplementary Information) is based on the static tunnelling rate[15,16] for an s-state with the binding energy of the highest occupied molecular orbital (HOMO) in OCS, taking saturation[23] into account and, importantly, including Stark shifts of both OCS and OCS$^+$ energy levels resulting from the interaction between the probe laser field, $\mathbf{E}_{probe}$, and the permanent and induced dipole moments. The Stark shifts lead to an effective ionization potential, $I_p^{eff}(\theta)$, used in the tunnelling model, given by:

$$
\begin{aligned}
I_p^{eff}(\theta) = {} & I_{p0} + (\mu^{OCS^+} - \mu^{OCS}) E_{probe} \cos\theta \\
& + \frac{1}{2} E_{probe}^2 [\{(\alpha_\parallel^{OCS} - \alpha_\parallel^{OCS^+}) - (\alpha_\perp^{OCS} - \alpha_\perp^{OCS^+})\} \cos^2\theta \\
& + (\alpha_\perp^{OCS} - \alpha_\perp^{OCS^+})]
\end{aligned}
\tag{1}
$$

Here $\mu^{OCS}(\mu^{OCS^+})$ is the permanent dipole moment of OCS (OCS$^+$), $\alpha_\parallel^{OCS}$ and $\alpha_\perp^{OCS}$ ($\alpha_\parallel^{OCS^+}$ and $\alpha_\perp^{OCS^+}$) are the polarizability components of OCS (OCS$^+$) parallel and perpendicular to the

[1]Department of Chemistry, Aarhus University, 8000 Aarhus C, Denmark, [2]Interdisciplinary Nanoscience Center (iNANO), Aarhus University, 8000 Aarhus C, Denmark, [3]Fritz-Haber-Institut der Max-Planck-Gesellschaft, Faradayweg 4-6, 14195 Berlin, Germany, [4]Lundbeck Foundation Theoretical Center for Quantum System Research, Department of Physics and Astronomy, Aarhus University, 8000 Aarhus C, Denmark. *e-mail: henriks@chem.au.dk; bojer@phys.au.dk.
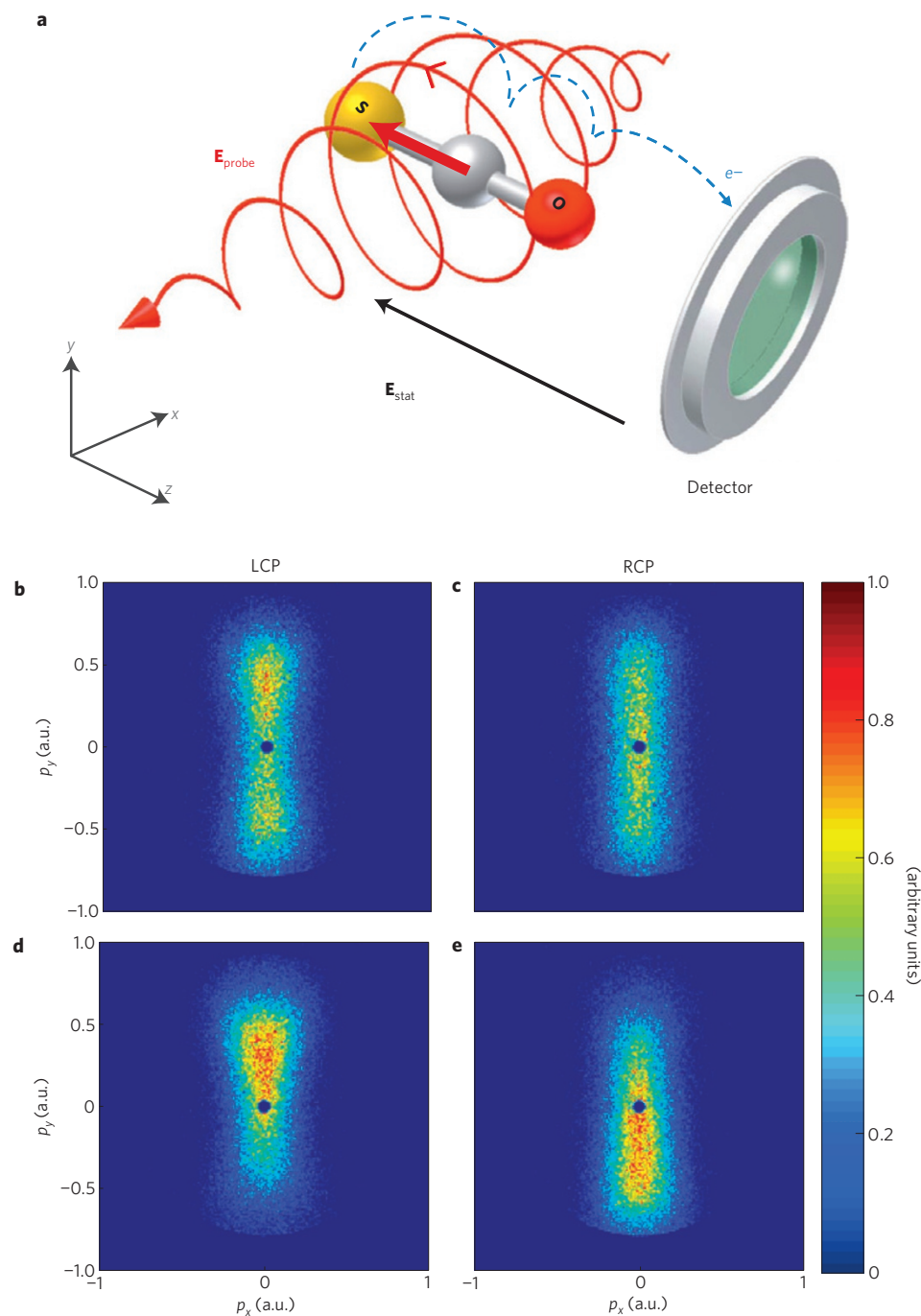
Figure 1 | Experimental photoelectron images from OCS. a, Schematic of the experimental set-up showing an OCS molecule oriented with its permanent dipole moment (bold red arrow) pointing in the direction of the static electric field, $\mathbf{E}_{stat}$. The LCP probe pulse ionizes the molecule and imparts an upward momentum to the freed electron resulting in recording on the upper part of the detector (see text for details). **b**, Two-dimensional momentum image of electrons produced when a (nearly) randomly oriented sample of OCS molecules are ionized by the LCP probe pulse. The polarization plane of the probe pulse is perpendicular to the image (detector). **c**, The same as in **b** but for a RCP probe pulse. **d,e**, As in **b** and **c** but with the OCS molecules oriented as in **a** by the alignment pulse polarized perpendicular to the image plane.

internuclear axis, I_{p0} is the ionization potential of OCS in the absence of any external fields and θ is the polar angle between the instantaneous direction of the circularly polarized probe field and the z axis (Fig. 1a). As the ionization (tunnelling) rate depends exponentially on the effective ionization potential[16], equation (1) shows directly that the oriented OCS molecules may have an asymmetric ionization probability depending on whether the probe field has a component parallel or antiparallel to the permanent dipole moment.

The situation is illustrated in Fig. 2a. It shows that $I_p^{\text{eff}}(\theta = \pi)$ is smaller than $I_p^{\text{eff}}(\theta = 0)$; that is, the ionization rate is larger for $\mathbf{E}_{probe}$ parallel rather than antiparallel to the permanent dipole moment. More generally, equation (1) states that I_p is smallest, and therefore ionization is most probable, for $\pi/2 \leq \theta \leq 3\pi/2$, corresponding to the half part of the optical period where the probe field has a component pointing towards the S-end. This angular dependence of the ionization probability causes a forward–backward asymmetry of the electron emission from the
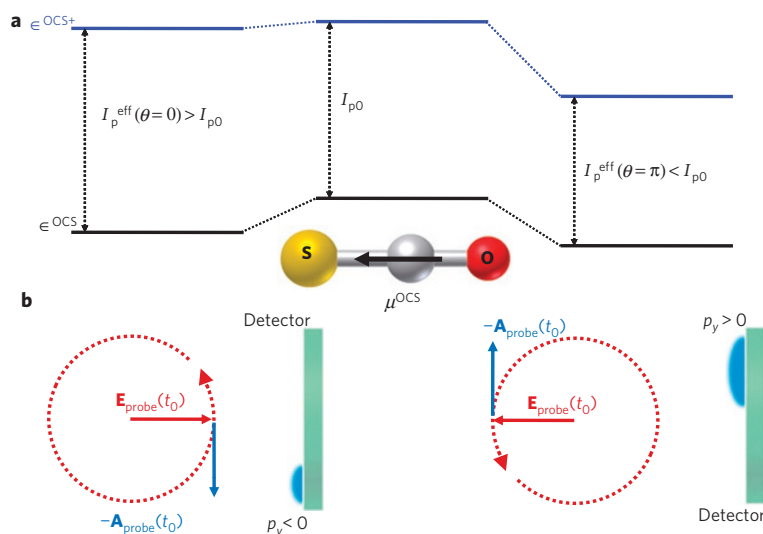
Figure 2 | Principle of OCS ionization and electron emission. a, Sketch of the effective ionization potential for $\mathbf{E}_{probe}$ antiparallel to μ^{OCS} (left), no $\mathbf{E}_{probe}$ (middle) and $\mathbf{E}_{probe}$ parallel to μ^{OCS} (right). The energy levels of OCS (OCS$^+$) are shown by bold black (blue) horizontal lines. **b**, Illustration of the momentum transfer to the electron owing to the force from the LCP probe field. In the tunnelling process, the electron escapes oppositely to the instantaneous direction of the probe field and acquires the final momentum, $-\mathbf{A}_{probe}(t_0)$. When $\mathbf{E}_{probe}$ is parallel (antiparallel) to μ^{OCS}, the electron receives an upward (downward) momentum; that is, $p_y > 0$ ($p_y < 0$). The ionization rate is higher in the parallel case, causing more upward than downward electrons.
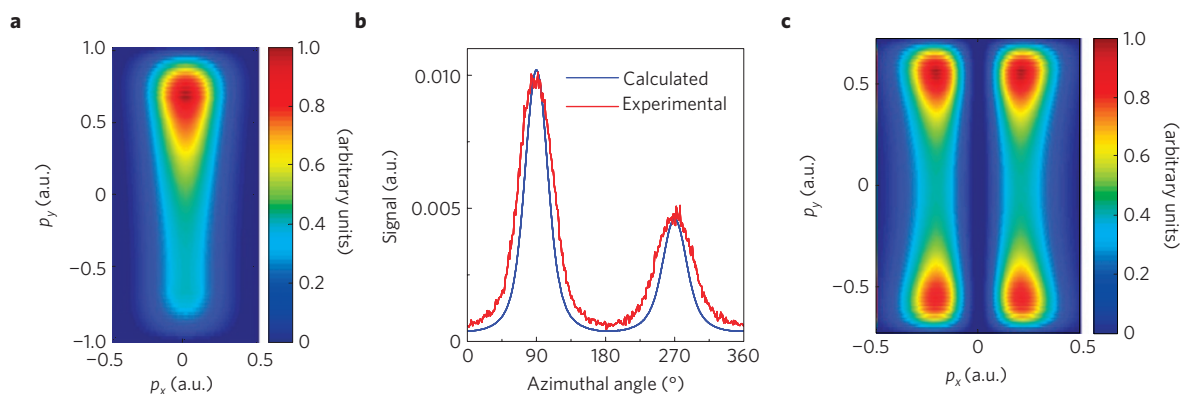

Figure 3 | Calculated photoelectron images and angular distributions. a, Calculated two-dimensional electron momentum distribution for ionization of one-dimensionally aligned and oriented OCS employing a LCP probe pulse similar to the one used in the experiment (Fig. 1d). **b**, Calculated (blue curve) angular distribution of the photoelectrons from the distribution in **a**. The red curve is the experimental angular distribution obtained from the image shown in Fig. 1d. **c**, Calculated two-dimensional electron momentum distribution for ionization from the HOMO and HOMO-1 of perfectly three-dimensionally aligned and oriented C_7H_5N employing a LCP probe pulse similar to the one used experimentally (Fig. 4e).

molecule with more electrons ejected when the field points in the direction of the permanent dipole moment. Before the electrons reach the detector they are subject to the force from the remaining part of the strong probe field, which leads to the final momentum distribution: $\mathbf{p}_f = -|e| \int_{t_0}^{\infty} \mathbf{E}_{probe}(t)\mathrm{d}t = -|e|\mathbf{A}_{probe}(t_0)$, where t_0 is the instant of ionization. The vector potential, $\mathbf{A}_{probe}(t)$, for LCP (RCP) advances the field by a phase of $\pi/2$ ($-\pi/2$) causing the forward–backward asymmetry in the ionization step to be transferred into an up–down asymmetry in the final momentum distribution (along the y direction, Fig. 1a). This is illustrated in Fig. 2b. The calculated momentum distribution, projected onto the plane corresponding to the detector, is shown in Fig. 3a for LCP probe pulses with the same characteristics as the experimental pulses. (The result with RCP pulses is identical except for having the opposite up–down asymmetry.) Focal volume effects are included[24] and an orientation of 80/20 based on the experimental findings is assumed. The similarity with the measurements (Fig. 1d) is clear. In particular, the theoretical up/total ratio of 65% compares very well

to the measured value (64%). A more quantitative comparison is provided in Fig. 3b, where the experimental and numerical angular distribution for LCP is plotted, obtained by radially integrating the images in Figs 2 and 3. The agreement is gratifying.

To illustrate the potential of our method for more complex molecules, experiments were conducted on benzonitrile (C_7H_5N). As for OCS the probe laser pulse removes only a single electron and causes no fragmentation. Consequently, MFPADs obtained by coincidence methods would not be possible. Again, Coulomb explosion imaging measurements confirmed that high degrees of alignment and orientation are achieved (Supplementary Information). Figure 4 shows the photoelectron distributions. Even without the alignment pulse, an up–down asymmetry (Fig. 4a,b) is observed. Although weak, it is more pronounced than in the case of OCS (Fig. 1b,c), which we ascribe to stronger one-dimensional orientation, induced by the static field[22], because C_7H_5N has a permanent dipole moment that is 6.3 times larger than that of OCS and the static field used is 35% larger. When the one-dimensional
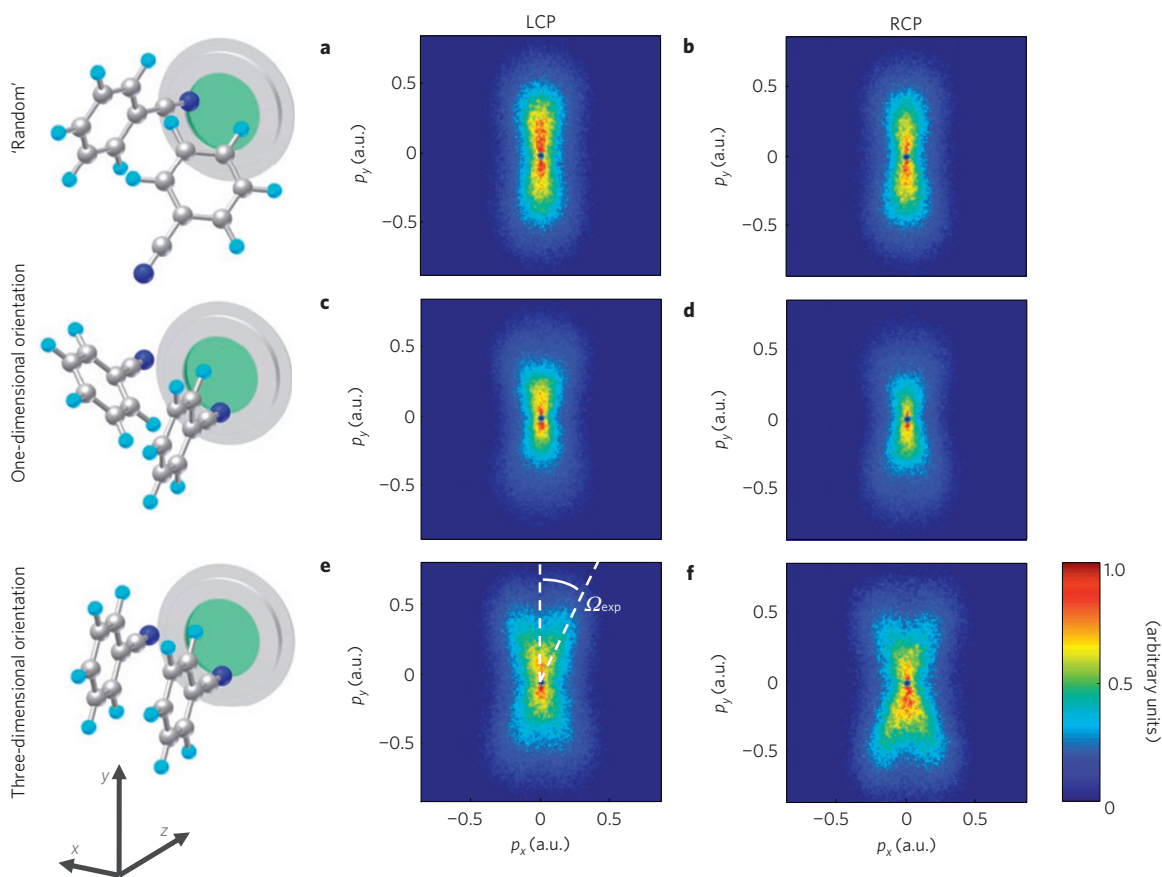
430

Figure 4 | Experimental photoelectron images from benzonitrile. a–f, Two-dimensional momentum image of electrons produced when C_7H_5N molecules are ionized by a LCP probe pulse (**a,c,e**) or a RCP probe pulse (**b,d,f**). In **a** and **b** the molecules are essentially randomly oriented (no alignment pulse). In **c** and **d** the molecules are one-dimensionally oriented (linearly polarized alignment pulse) and in **e** and **f** the molecules are three-dimensionally oriented (elliptically polarized alignment pulse). The intensity of the probe pulse is 1.2×10^{14} W cm^{-2}. In **e** the experimental off-the-nodal-plane angle, $\Omega_{exp} \simeq 18° \pm 1°$, is shown. See equation (2) for our analytical expression.

alignment pulse, linearly polarized along the static field axis, is included, the asymmetry increases (Fig. 4c,d) owing to stronger alignment and orientation. For LCP the up/total ratio is ~55%; for RCP it is ~44%. Unlike OCS, C_7H_5N is an asymmetric top molecule and the linearly polarized alignment pulse confines only the C–CN symmetry axis of the molecule, whereas the benzene ring remains free to rotate about this axis. Further confinement of the molecular plane, and thus three-dimensional alignment and orientation, is obtained by using an elliptically polarized alignment pulse[22,25] with the major axis along the static field axis and the minor axis vertical in the images. The total intensity, 7×10^{11} W cm^{-2}, is the same as for the linearly polarized pulse and the intensity ratio between the major and minor axis is 3:1. The resulting electron distributions (Fig. 4e,f) have essentially the same up–down asymmetry as in Fig. 4c,d (because the degree of one-dimensional alignment and orientation is essentially unchanged), but they exhibit striking new structures that are not seen in the PADs from one-dimensionally oriented molecules. In particular, electron emission in the polarization plane, coinciding with the nodal plane of the HOMO (and the HOMO-1), is suppressed. Such effects were predicted previously but never observed[26].

To explain the experimental findings for three-dimensionally oriented C_7H_5N, our theoretical model is extended. In contrast to OCS, the HOMO of C_7H_5N has a nodal plane (the molecular plane) and therefore, we model the initial state of C_7H_5N, perfectly three-dimensionally oriented in the way shown in the lower panel of Fig. 4, by a simple p_x orbital with the angular node in the polarization (y, z) plane and the p-lobes parallel to the x axis.

The presence of the nodal plane prevents electron emission in the polarization plane. This is observed in the calculated electron momentum distribution shown in Fig. 3c for LCP. Initial electron emission in the perpendicular direction is, however, possible and is incorporated by including a factor describing the momentum distribution in the x direction in the initial orbital (Supplementary Information). The slight asymmetry of the up/total ratio (52%) visible in Fig. 3c is still governed by laser-induced Stark shifts, as described for OCS, whereas the observed left–right splitting (along the x axis) of the momentum distribution projected on the detector plane results from the presence of the nodal plane. We obtain a closed analytical expression for the off-the-nodal-plane angle, Ω_{theo} (Fig. 4e), and at the intensity 1.2×10^{14} W cm^{-2},

$$\Omega_{theo} = \arctan(2\omega/\sqrt{\pi E_0 \kappa}) \simeq 18.8° \qquad (2)$$

with E_0 being the peak electric field of $\mathbf{E}_{probe}(t)$ and $\kappa = \sqrt{2I_{p0}}$, in good agreement with the experimental value, $\Omega_{exp} = 18° \pm 1°$ (Fig. 4e). The experimental observation of a non-zero electron signal in the polarization plane is partly due to non-perfect three-dimensional alignment of the molecule and possibly also due to a contribution from the HOMO-2 that has a nodal plane perpendicular to the laser polarization plane (Supplementary Information).

Our results show that MFPADs can be obtained for a broad range of species independent of whether one-dimensional or three-dimensional orientation is needed to fully fix a molecule in space. A particularly interesting extension is time-dependent phenomena where a pump pulse initiates a molecular transformation

or reaction. Strong-field ionization by circularly polarized femtosecond pulses, used here, is sensitive to the charge distribution of the valence electrons and could provide an efficient and ultrafast probe of, for instance, charge migration processes in molecules[27]. More generally, MFPADs using laser-oriented molecules will also be highly relevant for X-ray probing of molecular dynamics where detection of high-energy electrons can provide a direct structural diagnostics method to monitor the changing molecular species[28].

References

1. Gessner, O. *et al.* Femtosecond multidimensional imaging of a molecular dissociation. *Science* **311,** 219–222 (2006).
2. Bostedt, C. *et al.* Multistep ionization of argon clusters in intense femtosecond extreme ultraviolet pulses. *Phys. Rev. Lett.* **100,** 133401 (2008).
3. Tang, Y., Suzuki, Y., Horio, T. & Suzuki, T. Molecular frame image restoration and partial wave analysis of photoionization dynamics of NO by time-energy mapping of photoelectron angular distribution. *Phys. Rev. Lett.* **104,** 073002 (2010).
4. Suzuki, T. Femtosecond time-resolved photoelectron imaging. *Annu. Rev. Phys. Chem.* **57,** 555–592 (2006).
5. Meckel, M. *et al.* Laser-induced electron tunneling and diffraction. *Science* **320,** 1478–1482 (2008).
6. Bisgaard, C. Z. *et al.* Time-resolved molecular frame dynamics of fixed-in-space CS₂ molecules. *Science* **323,** 1464–1468 (2009).
7. Santra, R., Kryzhevoi, N. V. & Cederbaum, L. S. X-ray two-photon photoelectron spectroscopy: A theoretical study of inner-shell spectra of the organic para-aminophenol molecule. *Phys. Rev. Lett.* **103,** 013002 (2009).
8. Akagi, H. *et al.* Laser tunnel ionization from multiple orbitals in HCl. *Science* **325,** 1364–1367 (2009).
9. Shigemasa, E., Adachi, J., Oura, M. & Yagishita, A. Angular distributions of 1S-sigma photoelectrons from fixed-in-space N₂ molecules. *Phys. Rev. Lett.* **74,** 359–362 (1995).
10. Rolles, D. *et al.* Molecular-frame angular distributions of resonant CO:C(1s) Auger electrons. *Phys. Rev. Lett.* **101,** 263002 (2008).
11. Akoury, D. *et al.* The simplest double slit: Interference and entanglement in double photoionization of H₂. *Science* **318,** 949–952 (2007).
12. Schöffler, M. S. *et al.* Ultrafast probing of core hole localization in N₂. *Science* **320,** 920–923 (2008).
13. Yamazaki, M. *et al.* 3D mapping of photoemission from a single oriented H₂O molecule. *J. Phys. B* **42,** 052001 (2009).
14. Kumarappan, V. *et al.* Multiphoton electron angular distributions from laser-aligned CS₂ molecules. *Phys. Rev. Lett.* **100,** 093006 (2008).
15. Perelomov, A. M., Popov, V. S. & Terentev, M. V. Ionization of atoms in an alternating electric field. *Sov. Phys. JETP* **23,** 924–934 (1966).
16. Ammosov, M. V., Delone, N. B. & Krainov, V. P. Tunnel ionization of complex atoms and of atomic ions in an alternating electromagnetic field. *Sov. Phys. JETP* **64,** 1191–1194 (1986).
17. Friedrich, B. & Herschbach, D. Enhanced orientation of polar molecules by combined electrostatic and nonresonant induced dipole forces. *J. Chem. Phys.* **111,** 6157–6160 (1999).
18. Holmegaard, L. *et al.* Laser-induced alignment and orientation of quantum-state-selected large molecules. *Phys. Rev. Lett.* **102,** 023001 (2009).
19. Stapelfeldt, H. & Seideman, T. Colloquium: Aligning molecules with strong laser pulses. *Rev. Mod. Phys.* **75,** 543–557 (2003).
20. Filsinger, F. *et al.* Quantum-state selection, alignment, and orientation of large molecules using static electric and laser fields. *J. Chem. Phys.* **131,** 064309 (2009).
21. Keldysh, L. V. Ionization in the field of a strong electromagnetic wave. *Sov. Phys. JETP* **20,** 1307–1314 (1965).
22. Nevo, I. *et al.* Laser-induced 3D alignment and orientation of quantum state-selected molecules. *Phys. Chem. Chem. Phys.* **11,** 9912–9918 (2009).
23. Tong, X. M. & Lin, C. D. Empirical formula for static field ionization rates of atoms and molecules by lasers in the barrier-suppression regime. *J. Phys. B* **38,** 2593–2600 (2005).
24. Wang, P., Sayler, A. M., Carnes, K. D., Esry, B. D. & Ben-Itzhak, I. Disentangling the volume effect through intensity-difference spectra: Application to laser-induced dissociation of H₂⁺. *Opt. Lett.* **30,** 664–666 (2005).
25. Larsen, J. J., Hald, K., Bjerre, N., Stapelfeldt, H. & Seideman, T. Three dimensional alignment of molecules using elliptically polarized laser fields. *Phys. Rev. Lett.* **85,** 2470–2473 (2000).
26. Kjeldsen, T. K., Bisgaard, C. Z., Madsen, L. B. & Stapelfeldt, H. Influence of molecular symmetry on strong-field ionization: Studies on ethylene, benzene, fluorobenzene, and chlorofluorobenzene. *Phys. Rev. A* **71,** 013418 (2005).
27. Kuleff, A. I. & Cederbaum, L. S. Charge migration in different conformers of glycine: The role of nuclear geometry. *Chem. Phys.* **338,** 320–328 (2007).
28. Krasniqi, F. *et al.* Imaging molecules from within: Ultrafast angstrom-scale structure determination of molecules via photoelectron holography using free-electron lasers. *Phys. Rev. A* **81,** 033411 (2010).

Author contributions

L.H., J.L.H, L.K., S.L.K., H.S., F.F., J.K. and G.M. designed and carried out experiments. D.D., M.A-S., C.P.J.M. and L.B.M. developed the theory. All authors were involved in the completion of the manuscript.